

# NJC

Accepted Manuscript



This is an *Accepted Manuscript*, which has been through the Royal Society of Chemistry peer review process and has been accepted for publication.

*Accepted Manuscripts* are published online shortly after acceptance, before technical editing, formatting and proof reading. Using this free service, authors can make their results available to the community, in citable form, before we publish the edited article. We will replace this *Accepted Manuscript* with the edited and formatted *Advance Article* as soon as it is available.

You can find more information about *Accepted Manuscripts* in the [Information for Authors](#).

Please note that technical editing may introduce minor changes to the text and/or graphics, which may alter content. The journal's standard [Terms & Conditions](#) and the [Ethical guidelines](#) still apply. In no event shall the Royal Society of Chemistry be held responsible for any errors or omissions in this *Accepted Manuscript* or any consequences arising from the use of any information it contains.

## Universal degradation performances of high-efficiency AgBr/Ag<sub>2</sub>CO<sub>3</sub> photocatalyst under visible light and mechanism insight

Lu Yin<sup>a</sup>, Zhen Wang<sup>b</sup>, Lian Lu<sup>a</sup>, Xiankai Wan<sup>a</sup>, Huixiang Shi<sup>a\*</sup>

a. Department of Environmental Engineering, Zhejiang University, Hangzhou 310058,

PR China.

b. Environmental Science Research & Design Institute of Zhejiang Province. Hangzhou 310027, PR China

**Corresponding author at:** Zhejiang University, Department of Environmental Engineering, No. 388, Yuhangtang Road, Hangzhou, Zhejiang 310058, China.

Tel: +86-0571-81021986; Fax: +86-0571-81021989; E-mail: vic@zju.edu.cn(HX.Shi).

**Abstract:** High-efficiency visible-light-driven AgBr/Ag<sub>2</sub>CO<sub>3</sub> photocatalyst has been synthesized via a simple ion-exchange method. The textural, morphologies and optical properties of the photocatalysts were characterized by X-ray diffraction (XRD), scanning electron microscopy (SEM), nitrogen adsorption-desorption isotherms and UV-vis diffuse reflectance spectra (DRS). The prepared composite exhibited excellent photocatalytic efficiency for the degradation of methyl orange (MO), tetracycline (TC) and bisphenol A (BPA) under visible light irradiation ( $\lambda > 420$  nm). Compared to pure Ag<sub>2</sub>CO<sub>3</sub>, AgBr/Ag<sub>2</sub>CO<sub>3</sub> exhibited much higher photocatalytic activity and stability. The quenching effects of different scavengers and electron spin resonance (ESR) analysis suggest that holes and  $\bullet\text{O}_2^-$  were the main reactive species

responsible for the pollutant degradation and holes played the leading role. Two electron reaction processes were verified in the AgBr/Ag<sub>2</sub>CO<sub>3</sub> photocatalytic system on the basis of ESR and X-ray photoelectron spectroscopy (XPS). Thus, the two-stage photocatalytic mechanism was proposed.

**Keywords :** AgBr/Ag<sub>2</sub>CO<sub>3</sub>; Photocatalysis; Degradation; Reaction mechanism

## 1. Introduction

A variety of chemical substances are released into the water environment and giving cause for concern. As a potential green technology with the ability to decompose organic pollutants into inorganic substances, photocatalysis has attracted increasing attention.<sup>1-3</sup> So far, TiO<sub>2</sub> is believed to be the most widely used photocatalyst for its superiority in oxidation capacity, nontoxicity, and long-term stability.<sup>4</sup> However, TiO<sub>2</sub> can only be activated by wavelengths in the near-UV region (4% of the solar spectrum), which limits its photocatalytic activity. Thus, great effort has been devoted to develop novel photocatalysts which could exhibit high activity under visible light irradiation.<sup>5</sup> Among them, Ag-based photocatalysts are emerging as a promising candidate due to their excellent visible light-responsive photoelectrochemical properties.<sup>6</sup> In 2010, Ye et al.<sup>7</sup> reported a novel Ag<sub>3</sub>PO<sub>4</sub> photocatalyst

with extremely high photocatalytic efficiency under visible-light illumination which inspired the study of silver oxosalts.<sup>8</sup>  $\text{Ag}_2\text{CO}_3$  was then found to be another silver oxosalt with magnificent performance on organic pollutant degradation and disinfection which have drawn a lot of attention.<sup>9-11</sup> However, it should be noted that  $\text{Ag}_2\text{CO}_3$  is slightly soluble which reduces its structural stability in aqueous solution. Moreover, it suffered from photocorrosion leading to serious deactivation in recycle experiments which hinder its practical application.<sup>12</sup> Therefore, it is a crucial task to improve its stability while maintains the excellent photocatalytic performance.

Recently, construction of heterojunctions on the basis of silver halide ( $\text{AgX}$ ) has found to be an effective way for improving the original photocatalytic activity and stability of photocatalysts. It was reported that after coupling with  $\text{AgX}$ , the activity and stability of  $\text{Ag}_2\text{CO}_3$  was improved.<sup>13,14</sup> In the  $\text{AgBr}/\text{Ag}_2\text{CO}_3$  system, the hybrid composite displayed much higher photocatalytic activity than single  $\text{AgBr}$  or  $\text{Ag}_2\text{CO}_3$ , and the degradation efficiency still remained 93.4% after 4 cycling runs.<sup>15</sup> However, the published works mainly focused on the synthesis and property evaluation of the novel photocatalysts. The underlying mechanism of stability and activity enhancement for  $\text{AgBr}/\text{Ag}_2\text{CO}_3$  system was not studied systemically. No consensus has

been achieved on the photocatalytic oxidation process and mechanism.<sup>14</sup>  
<sup>15</sup> What is the role of AgBr playing in the coupled system? What is specific electron transfer process in the AgBr/Ag<sub>2</sub>CO<sub>3</sub> photocatalyst during the illumination? What is the main oxidant of pollutant in AgBr/Ag<sub>2</sub>CO<sub>3</sub> system? In addition, most scientific works study focused on the decomposition of dye molecules for Ag<sub>2</sub>CO<sub>3</sub>-based photocatalyst,  
<sup>16-18</sup> few attempts have been made to study the degradation of other pollutants. Therefore, further research and discussion are required.

In this work, to fully understand the photocatalytic process and mechanism of AgBr/Ag<sub>2</sub>CO<sub>3</sub> system, a comprehensive study was conducted. Three kinds of typical organic compounds, including methyl orange (MO, azo dye), tetracycline (TC, typical antibiotic) and bisphenol A [2, 2-bis (4-hydroxyphenyl)propane, BPA, endocrine disrupting compound] are selected as model substrates to evaluate the universal degradation ability of the photocatalyst. The important roles of AgBr in the complex system on the aspect of light adsorption, photocatalytic performance as well as stability enhancement were investigated and analyzed on the basis of UV-vis adsorption spectra, degradation measurements, photoelectrochemistry and cycle experiments. As the free radical and hole scavenging experiment may lead to change in mechanism,<sup>19</sup> electron spin resonance (ESR) were adopted to provide

direct and undisputed evidence to support the existence of  $\bullet\text{O}_2^-$ . Besides, the phenomenon of lagged generation of  $\bullet\text{O}_2^-$  was discussed for the first time and the main reactive oxidative species responsive for photocatalytic degradation of aqueous organic pollutants were revealed. Finally, to clarify the electron transfer route in the photocatalytic process during reaction, a two-stage photocatalytic reaction mechanism of AgBr/Ag<sub>2</sub>CO<sub>3</sub> under visible light was put forward.

## 2. Experimental

### 2.1 Synthesis

The synthesis of Ag<sub>2</sub>CO<sub>3</sub> was achieved by a simple precipitation reaction as reported elsewhere.<sup>20</sup> 0.1 M AgNO<sub>3</sub> aqueous solution was added to a beaker at ice-water bath condition and 0.05 M NaHCO<sub>3</sub> was added drop by drop. The mixture was stirred for 45 min and then filtered. The obtained light yellow green precipitations were washed with distilled water and alcohol for several times to dissolve any unreacted raw materials and dried at 50 °C for 8 h in the dark.

The AgBr/Ag<sub>2</sub>CO<sub>3</sub> heterojunctions were prepared by an ion-exchange method. Initially, 500 mg as-prepared Ag<sub>2</sub>CO<sub>3</sub> samples were dispersed in 20 mL distilled water by ultrasound. Subsequently, 10 mL NaBr solution with different concentration was dropped into the Ag<sub>2</sub>CO<sub>3</sub> suspension. After magnetic stirring for 2 h, the precipitations were

collected by filtration. The obtained mixtures were washed with distilled water and alcohol for several times and then dried at 50 °C for 8 h in the dark. In this work, the molar ratios of added Br/ original C were controlled to 20%, 40%, 60% and 80%, respectively. And those final samples were labeled as AgBr/Ag<sub>2</sub>CO<sub>3</sub>-20%, AgBr/Ag<sub>2</sub>CO<sub>3</sub>-40%, AgBr/Ag<sub>2</sub>CO<sub>3</sub>-60% and AgBr/Ag<sub>2</sub>CO<sub>3</sub>-80%, respectively.

For comparison, AgBr was synthesized by simple precipitation method according to a reported study.<sup>21</sup>

## 2.2 Characterization

X-ray diffraction (XRD, PANalytical X'Pert Pro) were carried out with Cu-K $\alpha$  radiation( $\lambda=0.154$  nm) in the  $2\theta$  range of 10-80°. X-ray tube voltage and current were 40 kV and 40 mA, respectively. The total Ag and Br content in the samples was determined with X-ray fluorescence spectroscopy (XRF, ARL ADVANT'X IntelliPowerTM, Thermo Fisher Scientific). Morphologies of the photocatalysts were studied by scanning electron microscopy (SEM, FEI SIRON) with an acceleration voltage of 25 kV. N<sub>2</sub> adsorption-desorption isotherm at 77K was measured on a BeiShiDe 3H-2000PS2 instrument. The specific surface area was calculated according to the Brunauer-Emmett-Teller (BET) model and the pore size distributions were analyzed using the Barrett-Joyner-Halenda (BJH) method from the desorption branch of the

$N_2$  adsorption-desorption isotherm. The UV-vis diffuse reflectance spectra was investigated on a UV-vis spectrophotometer (TU-1901, Pgeneral) equipped with an integrating sphere in the range of 230-850 nm using  $BaSO_4$  as the reflectance standard. X-ray photoelectron spectroscopy (XPS) analysis was conducted on an Escalab 250Xi photoelectron spectrometer (Thermo Fisher Scientific). Electron spin resonance (ESR) was obtained using a JES FA200 electron paramagnetic resonance spectrometer (JEOL). The photocurrent-time dependent experiments were carried out with an electrochemical workstation (CHI 660D) in a conventional three-electrode cell with a quartz window. The catalyst sample was drop-cast on ITO conducting glass with a fixed area of  $0.5 \text{ cm}^2$ . The as-prepared  $Ag_2CO_3$  or  $AgBr/Ag_2CO_3$  film was set as working electrode while a platinum sheet and an  $Ag/AgCl$  electrode were used as counter electrode and reference electrode, respectively. The measurement on  $Ag_2CO_3$  and  $AgBr/Ag_2CO_3$  at open circuit potential (OCV) were performed in  $0.1 \text{ M Na}_2SO_4$  solution under chopped illumination with 60s light on/off cycles.

### 2.3 Photocatalytic evaluation

The photocatalytic activity of the as-prepared samples was evaluated by degradation of MO (20 mg/L), BPA (10 mg/L) and TC (10 mg/L) under visible light. In a typical reaction, 100 mg of the as-prepared

photocatalyst was added into 100 mL of pollutant solution. All photocatalytic degradation experiments were carried out in a double-walled reactor with water coolant. A 300 W Xe lamp with a 420 nm cut off filter was positioned above the reactor as the visible light source. The photocatalyst was dispersed under sonication for several minutes before constant magnetic stirred for 45 min in the dark to reach adsorption-desorption equilibrium. During the photocatalytic reaction, samples were taken and centrifuged (10000 rpm, 5 min) to obtain pollutant solution without photocatalyst. The concentration of MO and TC was determined by a UV-vis spectrophotometer (TU-1800PC, Pgeneral) at 461 and 367 nm. The concentration of BPA was determined by HPLC (LC-2010A HT, Shimadzu) equipped with UV-vis detector and an Inertsil ODS-SP separation column (5  $\mu$  m, 4.6 $\times$ 150mm). The elution was monitored at 276 nm. The mobile phase was a mixture of acetonitrile and water (65/35, v/v) which was pumped at a flow rate of 1.0 mL/min. And  $C/C_0$  was used as evaluation of degradation where  $C$  was the pollutant concentration of the taken samples while  $C_0$  was the initial concentration. The total organic carbon (TOC) was measured to reveal the mineralization of the pollutants. TOC of the sample solution was detected with a Shimadzu TOC analyzer (TOC-V CPH).

For stability test of photocatalysts, the cycling runs were conducted

for five times. At the end of each cycle, catalysts were collected by centrifugation and washed by deionize water. Then fresh pollutant solution was added to the used catalysts as the beginning of the next cycle.

### 3. Result and discussion

#### 3.1 Textural, morphology and optical properties

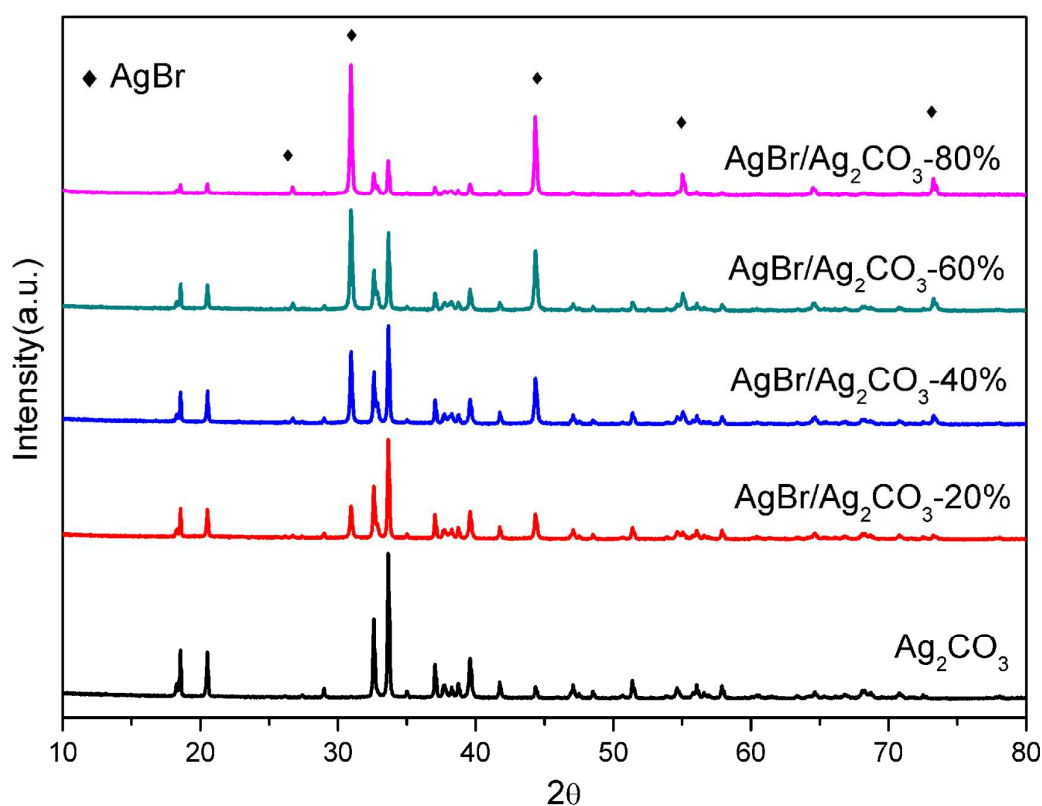


**Fig.1 XRD patterns of as-prepared Ag<sub>2</sub>CO<sub>3</sub> and AgBr/Ag<sub>2</sub>CO<sub>3</sub> with different AgBr contents.**

Fig.1 displays the XRD patterns of the as-prepared AgBr/Ag<sub>2</sub>CO<sub>3</sub> hybrid photocatalysts with different AgBr content as well as pure Ag<sub>2</sub>CO<sub>3</sub>. The result indicates that compare with the pure Ag<sub>2</sub>CO<sub>3</sub> (JCPDS 26-0339),

several additional peaks were discerned in the patterns of the hybrids which could be indexed to the characteristic peaks of AgBr (JCPDS 06-0438). Besides, no peaks from other substance were observed such as Ag and Ag<sub>2</sub>O thus confirms the synthesis of AgBr/Ag<sub>2</sub>CO<sub>3</sub> hybrid photocatalysts. As exhibited in the patterns, the intensities of the characteristic peaks of AgBr got stronger along with the increasing molar ratio of AgBr in the hybrids while those of Ag<sub>2</sub>CO<sub>3</sub> decreased. For the pattern of pure Ag<sub>2</sub>CO<sub>3</sub>, all the diffraction peaks can be indexed to the crystalline phase of Ag<sub>2</sub>CO<sub>3</sub>. The results demonstrate that AgBr/Ag<sub>2</sub>CO<sub>3</sub> hybrid photocatalysts can be synthesized by anion-exchange reaction. To investigate the real amount of AgBr in the hybrids, XRF elemental analysis was used. Based on XRF elemental analysis and the XRD data, we determined the actual ratio of AgBr/Ag<sub>2</sub>CO<sub>3</sub> for AgBr/Ag<sub>2</sub>CO<sub>3</sub>-20%, 40%, 60% and 80% are 22.3%, 52.2%, 84.0% and 137.1%, respectively. The experimental results are close to the theoretical amount and the results are displayed in Table 1.

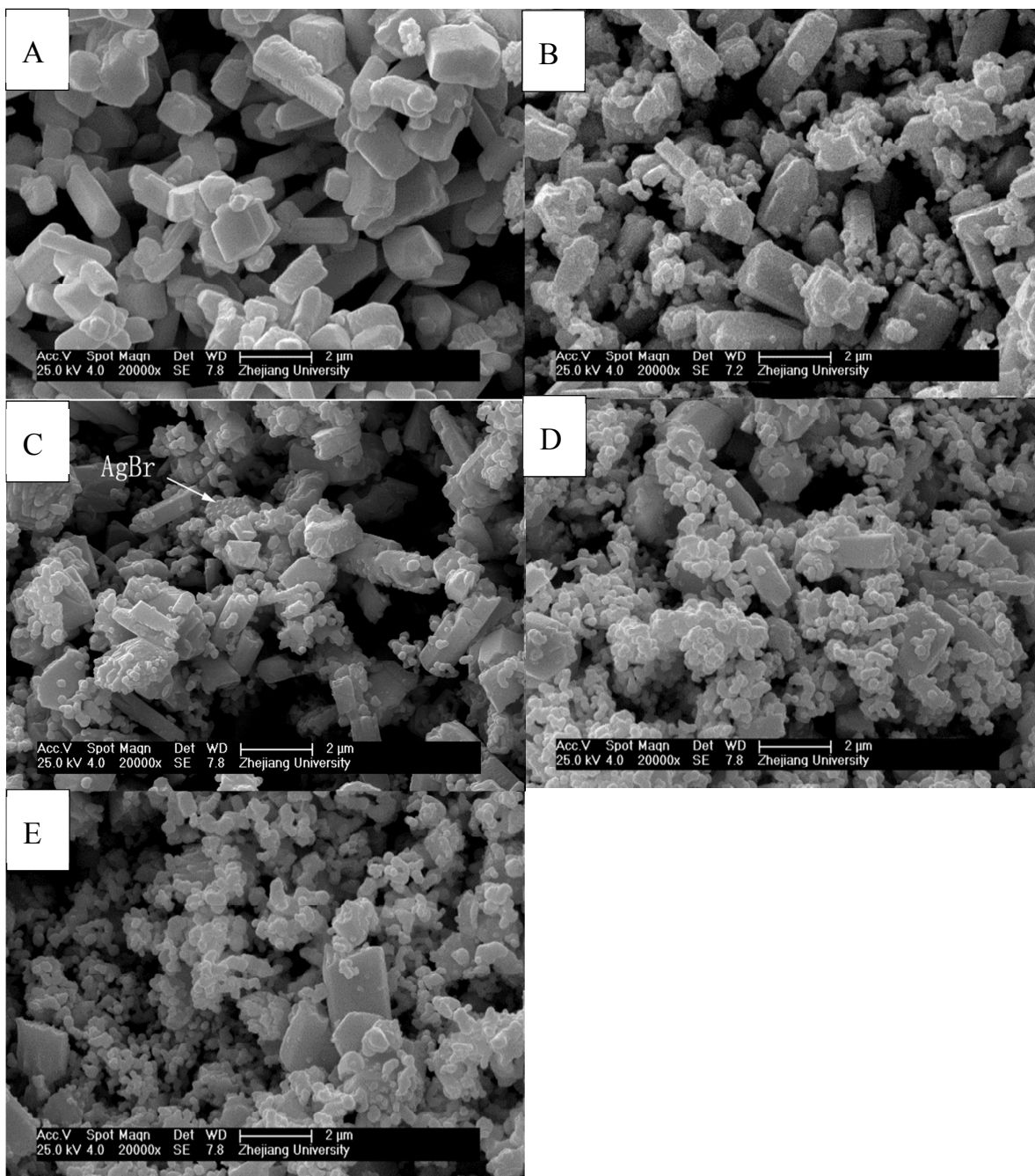


**Fig.2 SEM image of pure  $\text{Ag}_2\text{CO}_3$  (A),  $\text{AgBr}/\text{Ag}_2\text{CO}_3$ -20% (B),  $\text{AgBr}/\text{Ag}_2\text{CO}_3$ -40% (C),  $\text{AgBr}/\text{Ag}_2\text{CO}_3$ -60% (D) and  $\text{AgBr}/\text{Ag}_2\text{CO}_3$ -80% (E).**

To investigate the morphology and particle size of the synthesized samples, SEM was performed and the images are displayed in Fig. 2. It is

observed that  $\text{Ag}_2\text{CO}_3$  samples were prism-like particles with the diameter of 0.5-1.2 $\mu\text{m}$  and length of 1.3-2.5 $\mu\text{m}$  in Fig 2A. They have clean, smooth surfaces. After reacted with NaBr, the surface became rough due to the formation of small AgBr particles on the surface of  $\text{Ag}_2\text{CO}_3$  crystal which can clearly been seen in Fig 2C. The particles are 0.1-0.2 $\mu\text{m}$  in size with irregular shape. Apart from the particles assembled on the surface of  $\text{Ag}_2\text{CO}_3$ , a large number of AgBr particles existed around the  $\text{Ag}_2\text{CO}_3$  crystal. This can be explained as follows: the  $\text{Ag}_2\text{CO}_3$  is slightly soluble thus as the reaction goes, more and more  $\text{Ag}^+$  dissolves in the aqueous solution and form the AgBr precipitation. The amount of AgBr particles obviously grew when the mole ratio of AgBr increased as illustrated in Fig 2B-E. Only a few  $\text{Ag}_2\text{CO}_3$  particles can be found in AgBr/ $\text{Ag}_2\text{CO}_3$ -80% and small AgBr particles were dominant.

**Table 1 Theoretical and actual AgBr/ $\text{Ag}_2\text{CO}_3$  percentage, specific surface area and pseudo-first-order rate constants (k) of different photocatalysts.**

photocatalyst	theoretical AgBr/ $\text{Ag}_2\text{CO}_3$ percentage(Br/C%)	actual AgBr/ $\text{Ag}_2\text{CO}_3$ percentage(Br/C%)	BET surface area ( $\text{m}^2/\text{g}$ )	k( $\text{min}^{-1}$ )
$\text{Ag}_2\text{CO}_3$	-	-	1.444	0.119
AgBr/ $\text{Ag}_2\text{CO}_3$ -20%	22.2	22.3	3.548	0.152
AgBr/ $\text{Ag}_2\text{CO}_3$ -40%	50	52.2	2.299	0.224
AgBr/ $\text{Ag}_2\text{CO}_3$ -60%	85.7	84.0	2.110	0.397
AgBr/ $\text{Ag}_2\text{CO}_3$ -80%	133.3	137.1	1.772	0.312

The Brunauer-Emmett-Teller (BET) specific surface areas of the prepared samples were studied by nitrogen sorption. The results are displayed in Table 1. Specific surface areas of AgBr/Ag<sub>2</sub>CO<sub>3</sub> hybrids were larger than the pure Ag<sub>2</sub>CO<sub>3</sub>. It is attributed to the small AgBr particles formed on the Ag<sub>2</sub>CO<sub>3</sub> surface which enlarge the surface area significantly. This is confirmed by the results of SEM in Fig. 2. AgBr/Ag<sub>2</sub>CO<sub>3</sub>-20% possessed the largest specific surface area (3.548 m<sup>2</sup>/g) and as the AgBr content increased, the specific surface area decreased. In addition, N<sub>2</sub> adsorption and desorption isotherms and pore-size distributions calculated from desorption branch of the nitrogen isotherms by the BJH method were also measured (see Fig. SI 1). All samples display type III (Brunauer-Deming-Deming-Teller (BDDT) classification) isotherm, which characteristically indicates that weak interaction take place between N<sub>2</sub> molecules and the samples. The pore-size distributions of all the samples show mesopores with peak pore diameter at range of 2.68-4.53 nm confirming the formation of mesopores.

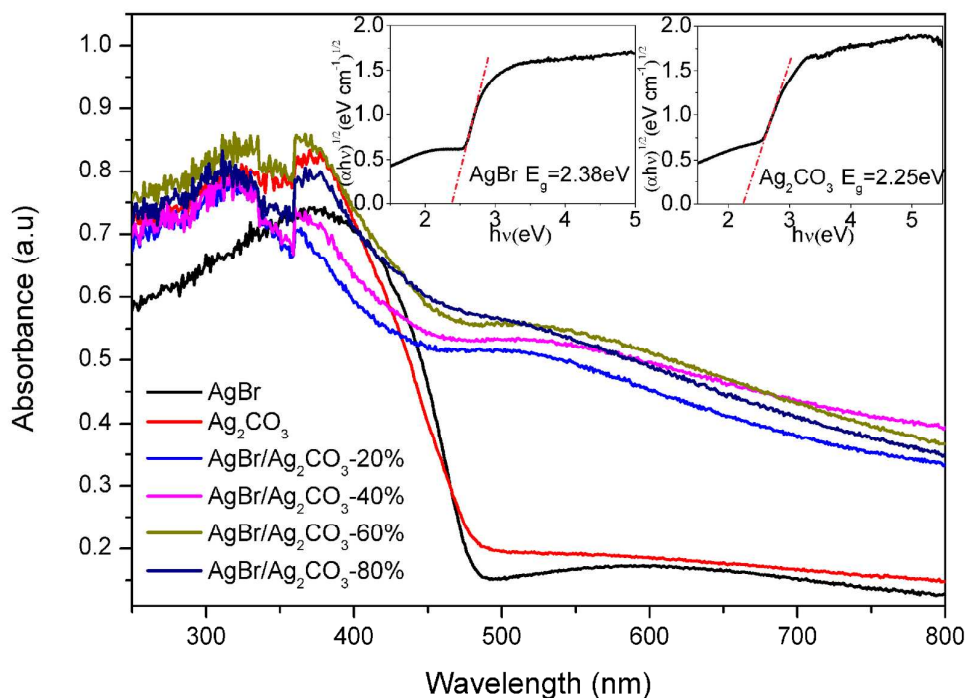


**Fig. 3** UV-vis absorption spectra of AgBr/Ag<sub>2</sub>CO<sub>3</sub> hybrids. The insets show the band gap evaluation for linear dependence of  $(\alpha hv)^{1/2}$  versus  $h\nu$  for the Ag<sub>2</sub>CO<sub>3</sub> and AgBr samples.

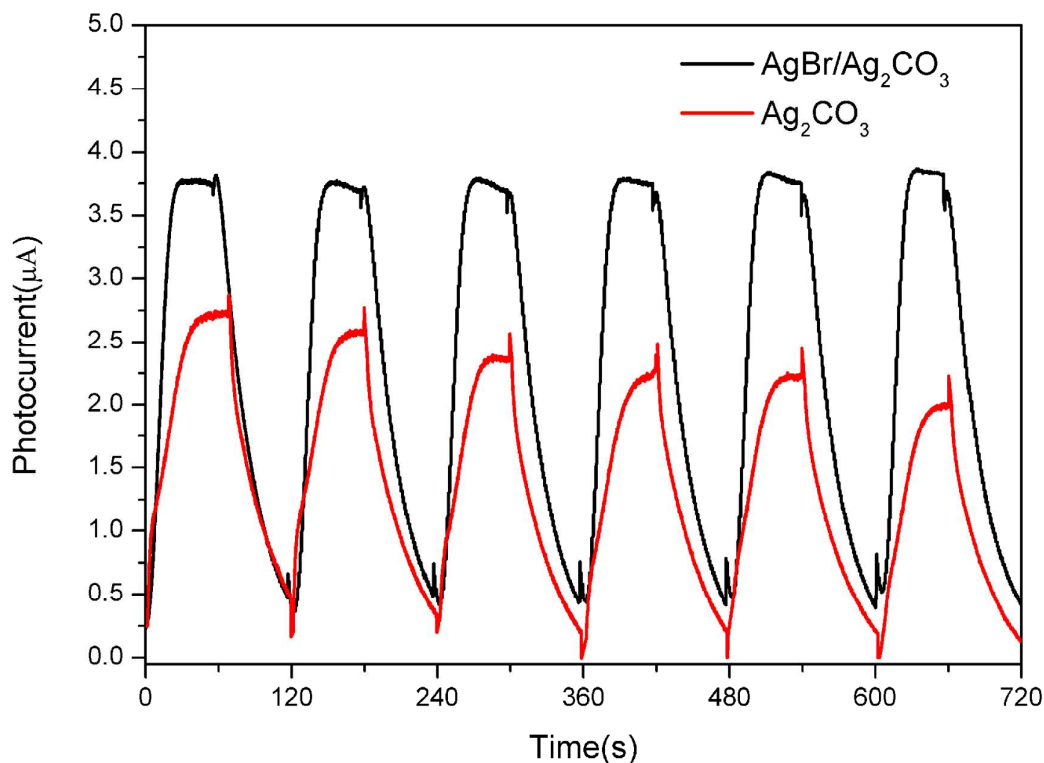
Fig.3 shows the UV-vis absorption spectra for pure Ag<sub>2</sub>CO<sub>3</sub>, AgBr and AgBr/Ag<sub>2</sub>CO<sub>3</sub> hybrids. The AgBr/Ag<sub>2</sub>CO<sub>3</sub> hybrids exhibited stronger absorption in visible-light region than Ag<sub>2</sub>CO<sub>3</sub>, and AgBr/Ag<sub>2</sub>CO<sub>3</sub>-60% had the strongest absorption. The overloading of AgBr might result in blocking the light for Ag<sub>2</sub>CO<sub>3</sub> particles which decreases the overall light absorbance. This result is consistent with the color changing of samples which alter from gray to black to gray when AgBr loading ratio increases. It is worth noting that the hybrids turned gray and dark while Ag<sub>2</sub>CO<sub>3</sub> and AgBr were both yellow precipitates. The reason can be the changing optical properties of the heterojunction as demonstrated by Xu et al.<sup>14</sup>.

Since the light harvest ability has great impact on photocatalytic performance, the strong absorption of AgBr/Ag<sub>2</sub>CO<sub>3</sub> hybrids in visible-light region is beneficial for the degradation of organic pollutants.

According to a previous study,<sup>20</sup> as indirect band gap semiconductors, the band gap of Ag<sub>2</sub>CO<sub>3</sub> can be determined by the following equation :

$\alpha h\nu = A(h\nu - E_g)^2$ , where  $\alpha$ ,  $h\nu$ , A and  $E_g$  are absorption coefficient, discrete photo energy, a constant related to the material, and band gap, respectively. For Ag<sub>2</sub>CO<sub>3</sub> and AgBr, the curves of  $(\alpha h\nu)^{1/2}$  versus  $(h\nu)$  are plotted in the insets of Fig.3. The band gaps of Ag<sub>2</sub>CO<sub>3</sub> and AgBr were estimated to be 2.25 eV and 2.38 eV by extrapolating the tangent line along  $h\nu$  axis.

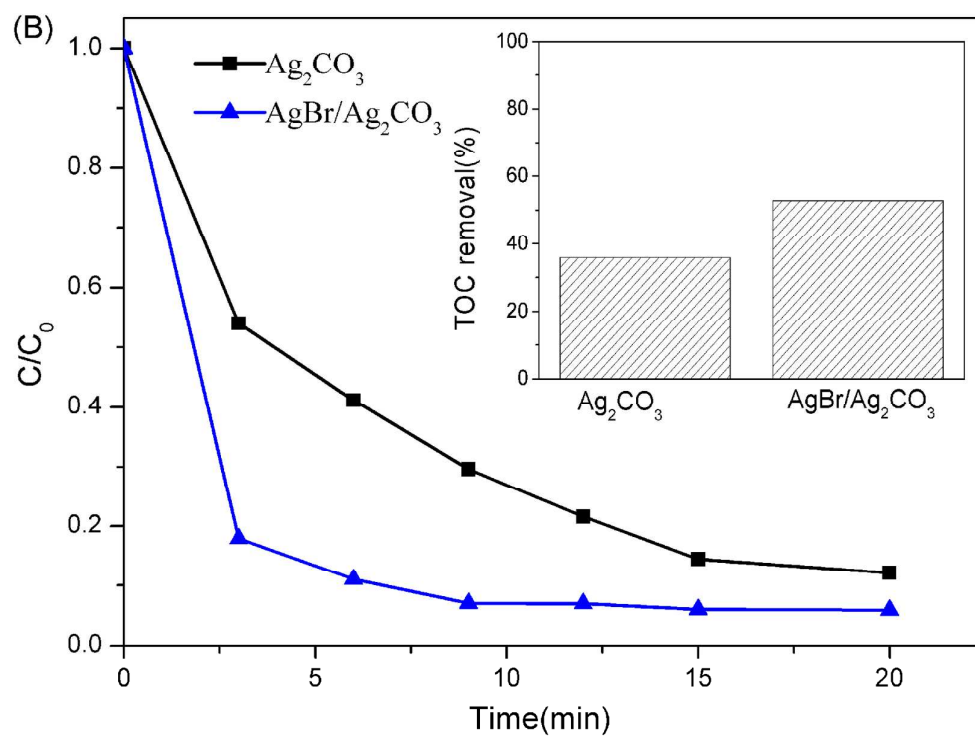
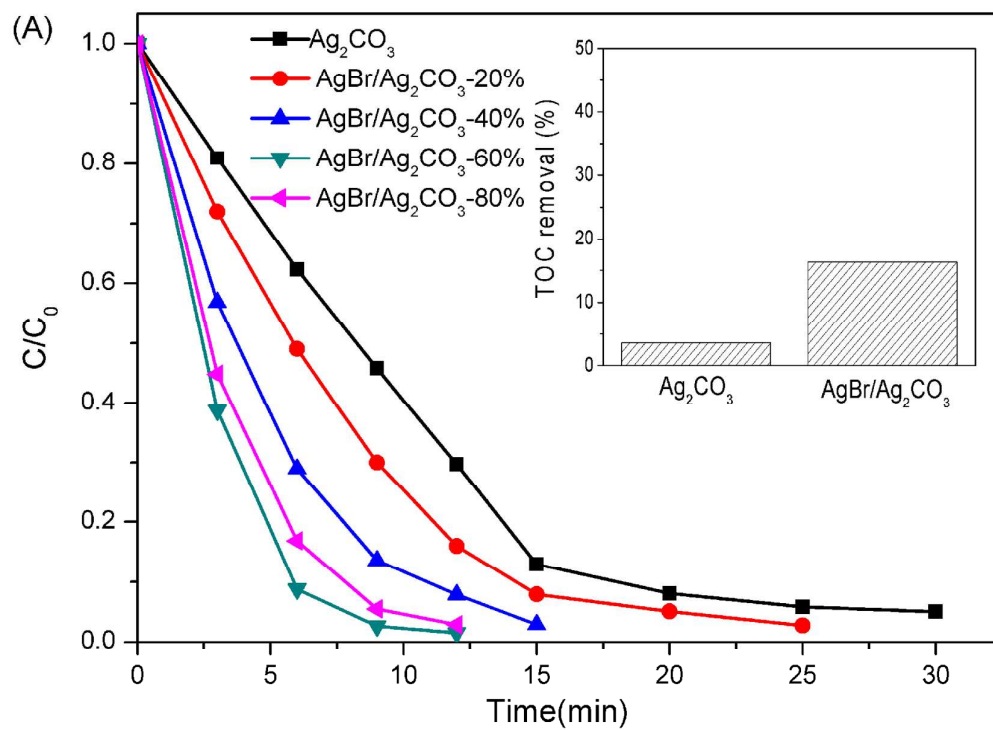
### 3.2 Photocurrent analysis



**Fig. 4** Photocurrent response of pure  $\text{Ag}_2\text{CO}_3$  and  $\text{AgBr}/\text{Ag}_2\text{CO}_3$ -60% samples.

Fig.4 shows the photocurrents of  $\text{Ag}_2\text{CO}_3$  and  $\text{AgBr}/\text{Ag}_2\text{CO}_3$  under visible light illumination ( $\lambda > 420 \text{ nm}$ ). It was obvious that compared with  $\text{Ag}_2\text{CO}_3$ , the  $\text{AgBr}/\text{Ag}_2\text{CO}_3$  exhibited higher photocurrent. This enhancement resulted from the increased visible absorption and higher electron and hole separation efficiency of  $\text{AgBr}/\text{Ag}_2\text{CO}_3$ ,<sup>13</sup> which lead to the rise quantity of separated photogenerated carriers. Besides, the maximum photocurrent value of  $\text{Ag}_2\text{CO}_3$  in each cycle decreased from  $2.7 \mu\text{A}$  to  $2.0 \mu\text{A}$  over time while that of  $\text{AgBr}/\text{Ag}_2\text{CO}_3$  maintained stable at  $3.8 \mu\text{A}$ . It could be inferred that  $\text{AgBr}/\text{Ag}_2\text{CO}_3$  possessed higher stabilization than pure  $\text{Ag}_2\text{CO}_3$ .

### 3.3 Photocatalytic activity of AgBr/Ag<sub>2</sub>CO<sub>3</sub>



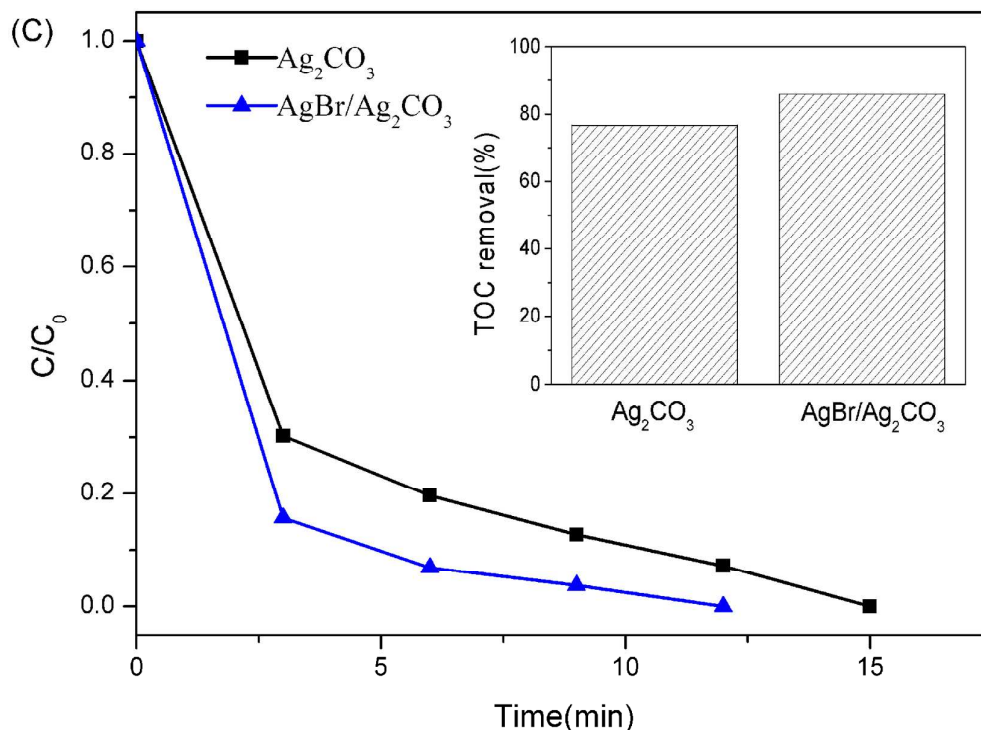


**Fig. 5** Variation of MO concentration against irradiation time using pure  $\text{Ag}_2\text{CO}_3$  and  $\text{AgBr}/\text{Ag}_2\text{CO}_3$  hybrids with different AgBr contents. The inset shows the TOC removal of MO in the presence of pure  $\text{Ag}_2\text{CO}_3$  and  $\text{AgBr}/\text{Ag}_2\text{CO}_3$ -60% composite after 30 min. (A) Variation of TC concentration (B) and BPA concentration (C) against irradiation time using pure  $\text{Ag}_2\text{CO}_3$  and  $\text{AgBr}/\text{Ag}_2\text{CO}_3$ -60% with the inset of TOC removal after 30 min.

The photocatalytic activities of pure  $\text{Ag}_2\text{CO}_3$  and  $\text{AgBr}/\text{Ag}_2\text{CO}_3$  hybrids with various AgBr content under visible light ( $\lambda > 420$  nm) irradiation were investigated by the degradation of aqueous MO. As shown in Fig. 5A, all the  $\text{AgBr}/\text{Ag}_2\text{CO}_3$  hybrids exhibited higher photocatalytic activities than pure  $\text{Ag}_2\text{CO}_3$  and the ratio of  $\text{AgBr}/\text{Ag}_2\text{CO}_3$  had a significant impact on the photodegradation performance. The photocatalytic degradation efficiency of MO increased with the AgBr

loading and achieved the highest with the AgBr content of 60%. Under the visible light irradiation, 97.3% of MO was decomposed after 9 min over AgBr/Ag<sub>2</sub>CO<sub>3</sub>-60% while only 54.2% of MO was degraded over Ag<sub>2</sub>CO<sub>3</sub> under the same condition. The linear relationship between ln(C<sub>0</sub>/C) and time are shown in Fig. SI 2, indicating that the photodegradation of MO follows pseudo-first-order kinetics. The apparent reaction rate constants (k) were calculated to quantitatively evaluate the reaction kinetics of different samples on degradation of MO. The results are displayed in Table 1. The value of k is in the order as follows: k(AgBr/Ag<sub>2</sub>CO<sub>3</sub>-60%) > k(AgBr/Ag<sub>2</sub>CO<sub>3</sub>-80%) > k(AgBr/Ag<sub>2</sub>CO<sub>3</sub>-40%) > k(AgBr/Ag<sub>2</sub>CO<sub>3</sub>-20%) > k(Ag<sub>2</sub>CO<sub>3</sub>). The photocatalyst AgBr/Ag<sub>2</sub>CO<sub>3</sub>-60% shows the largest k value of 0.397 min<sup>-1</sup>, which is about 3.3 times of the k for the pure Ag<sub>2</sub>CO<sub>3</sub> and 2.6 times of that for AgBr/Ag<sub>2</sub>CO<sub>3</sub>-20%. In addition, the surface area of AgBr/Ag<sub>2</sub>CO<sub>3</sub>-60% (2.110 m<sup>2</sup>/g) is smaller than AgBr/Ag<sub>2</sub>CO<sub>3</sub>-20% (3.548 m<sup>2</sup>/g), which indicates that specific surface area is not the crucial property that affects the photocatalytic ability in AgBr/Ag<sub>2</sub>CO<sub>3</sub> system. However, as the AgBr loading rose to 80%, a slight decrease in the photocatalytic activity of the hybrid was observed. The k value for AgBr/Ag<sub>2</sub>CO<sub>3</sub>-80% is 0.312 min<sup>-1</sup> which is smaller than that for AgBr/Ag<sub>2</sub>CO<sub>3</sub>-60%. This phenomenon existed in many photocatalytic

heterojunction systems<sup>22-24</sup> and was consistent with the result of the UV-vis DRS (Fig 3). The photocatalytic performance is depended on the production of separated photogenerated electrons and holes. In AgBr/Ag<sub>2</sub>CO<sub>3</sub> heterojunction system, when the AgBr content was below 60%, the AgBr nanoparticles were grown dispersedly on the surface of Ag<sub>2</sub>CO<sub>3</sub>. It is beneficial for the light adsorption. Moreover, the closely contacted interface area gained as the AgBr ratio rose which facilitated the separation of electron-hole pairs. However, when the AgBr content was up to 80%, the AgBr nanoparticles agglomerated and were isolated from Ag<sub>2</sub>CO<sub>3</sub> (Fig. 2e) which reduced the interface area and light adsorption thus leading to the decrease of photocatalytic activity. Furthermore, TOC removal percentage of MO over pure Ag<sub>2</sub>CO<sub>3</sub> and AgBr/Ag<sub>2</sub>CO<sub>3</sub>-60% after 30 min irradiation was monitored. The result is shown in the inset of Fig. 5A. The TOC removal percentage was 3.6% and 16.3% for pure Ag<sub>2</sub>CO<sub>3</sub> and AgBr/Ag<sub>2</sub>CO<sub>3</sub>-60%, respectively. AgBr/Ag<sub>2</sub>CO<sub>3</sub>-60% displayed higher mineralization ability than pure Ag<sub>2</sub>CO<sub>3</sub>. It is notable that the TOC removal percentage was significantly lower than the discoloration percentage of MO, indicating that the MO molecules needed much more effort to be completely mineralized than just be destroyed.<sup>25</sup>

To confirm the universal degradation ability of as-prepared

photocatalysts, photocatalytic activities toward TC and BPA were also evaluated in the presence of pure  $\text{Ag}_2\text{CO}_3$  and  $\text{AgBr}/\text{Ag}_2\text{CO}_3$ -60%. The degradation curves against irradiation time are shown in Fig. 5B and 5C. The TOC removal efficiency after 30 min illumination is illustrated in the inset. It is clear that  $\text{AgBr}/\text{Ag}_2\text{CO}_3$ -60% presented higher activity in both photocatalytic experiments. The TOC removal yields of pure  $\text{Ag}_2\text{CO}_3$  and  $\text{AgBr}/\text{Ag}_2\text{CO}_3$ -60% toward TC were 35.9% and 52.87%, respectively. The mineralization efficiency toward BPA reached 76.7% and 85.9% over pure  $\text{Ag}_2\text{CO}_3$  and  $\text{AgBr}/\text{Ag}_2\text{CO}_3$ -60% which was significantly greater than that toward MO and TC. In summary,  $\text{AgBr}/\text{Ag}_2\text{CO}_3$  composite exhibited excellent photocatalytic activity for the degradation of MO, TC and BPA, which suggested its potential for the application on degrading different organic pollutants in waste water. Besides, the mineralization efficiency varied by pollutants.

### 3.4 Stability of the photocatalysts

In addition to photocatalytic efficiency, the stability of a photocatalyst is one of the most important parameters for its application. Thus the stability of photocatalysts was further evaluated in five successive MO degradation experiments. The results are shown in Fig. 6. It was found that pure  $\text{Ag}_2\text{CO}_3$  exhibited significantly decreased photocatalytic performance after 1 run and lost activity in the fifth run.

On the contrary, AgBr/Ag<sub>2</sub>CO<sub>3</sub>-60% still maintains 90.4% of MO degradation in 20 min after 4 cycles, indicating the hybrid composite possessed higher stability.

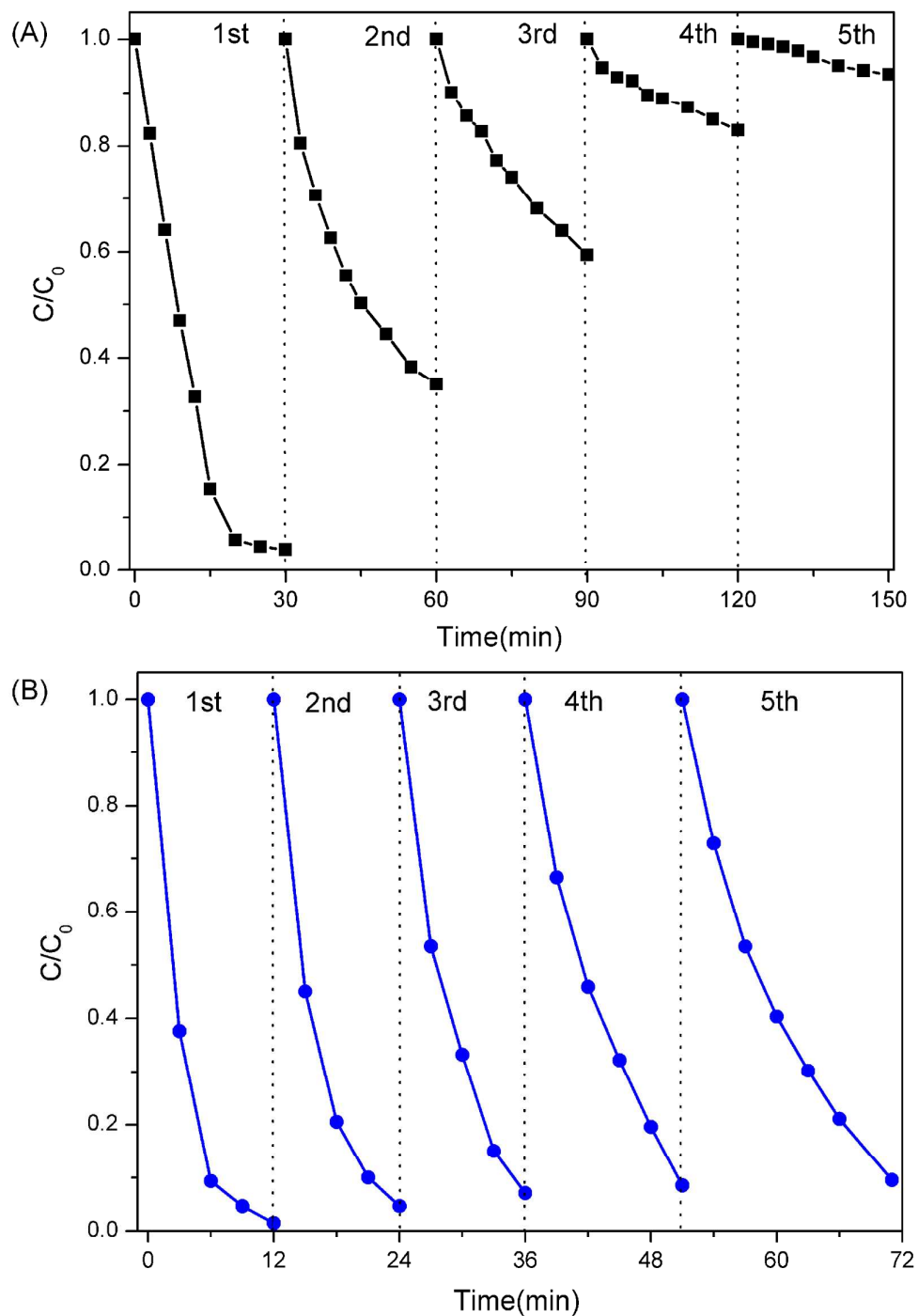


**Fig. 6** Cycling runs in the photodegradation of MO in the presence of pure  $\text{Ag}_2\text{CO}_3$  (A) and  $\text{AgBr}/\text{Ag}_2\text{CO}_3$ -60% composite under visible light.

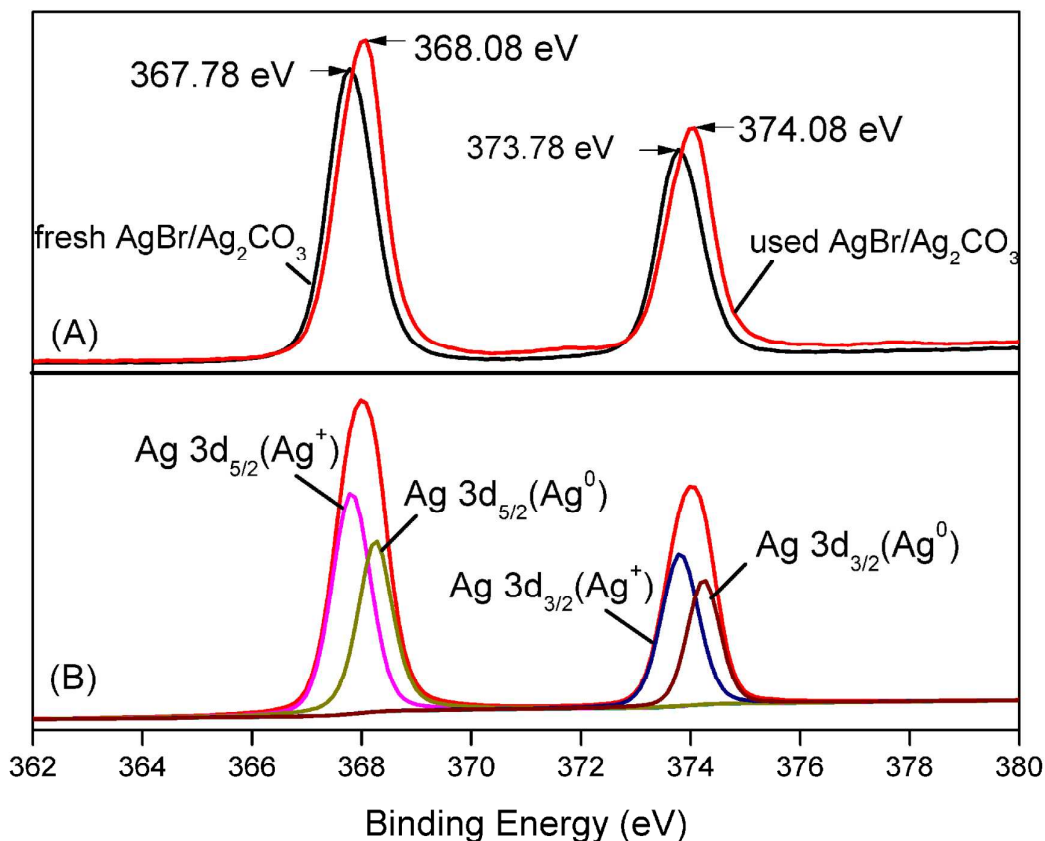


**Fig 7.** Ag3d XPS spectra of the fresh  $\text{AgBr}/\text{Ag}_2\text{CO}_3$ -60% composite and the used  $\text{AgBr}/\text{Ag}_2\text{CO}_3$ -60% composite after 1 recycling run (A) and fitting curve of the used  $\text{AgBr}/\text{Ag}_2\text{CO}_3$ -60% composite after 1 recycling run (B).

It's worth noting that during photocatalytic reaction,  $\text{AgBr}/\text{Ag}_2\text{CO}_3$ -60% composite turned black soon after illumination. We believed that metallic silver was formed during this period. To confirm the existence of metal silver, the used photocatalyst was collected and analyzed by XPS and XRD. The fresh  $\text{AgBr}/\text{Ag}_2\text{CO}_3$ -60% composite was analyzed as well. The XPS spectras are shown in Fig. 7. The peaks of fresh composite at 367.78 eV and 373.78 eV can be attributed to  $\text{Ag}^+$  of

AgBr and Ag<sub>2</sub>CO<sub>3</sub> indicating no existence of Ag<sup>0</sup>.<sup>26</sup> The peaks of used AgBr/Ag<sub>2</sub>CO<sub>3</sub>-60% composite shifted to 368.08 eV and 374.08 eV which was resulted from the formation of Ag<sup>0</sup>. The XPSPEAK software was used to separate the Ag<sup>+</sup> peaks and Ag<sup>0</sup> peaks. The result is displayed in Fig.7B. The weak peaks at 368.25 eV and 374.24 eV are attributed to Ag<sup>0</sup>.<sup>26</sup> The XRD patterns of the fresh and used AgBr/Ag<sub>2</sub>CO<sub>3</sub>-60% samples are shown in Fig. SI 4. Compared with the fresh composite, the used sample displayed significant higher intensity of diffraction peak at 38.1° which is assigned to the diffractions of Ag<sup>0</sup>. Hence, the existence of Ag NPs in used AgBr/Ag<sub>2</sub>CO<sub>3</sub>-60% composite was proved. According to the above results, Ag NPs was formed during the photocatalytic reaction. It was the Ag/AgBr/Ag<sub>2</sub>CO<sub>3</sub> system, rather than AgBr/Ag<sub>2</sub>CO<sub>3</sub> system, showing great stability in photocatalytic degradation performance.

Furthermore, theoretically the formation of Ag NPs can diminish the reduction of Ag<sup>+</sup>, leading to more stable Ag/Ag<sub>2</sub>CO<sub>3</sub> photocatalyst.<sup>27</sup> However, the Ag<sub>2</sub>CO<sub>3</sub> composite was unstable while AgBr/Ag<sub>2</sub>CO<sub>3</sub> composite exhibited much higher stability. Considering the relatively high solubility of Ag<sub>2</sub>CO<sub>3</sub> and much lower solubility of AgBr, we believe that to a certain extent, the enhanced stability of AgBr/Ag<sub>2</sub>CO<sub>3</sub> composite is achieved by the decrease of Ag<sub>2</sub>CO<sub>3</sub> dissolution resulting from the AgBr coating on Ag<sub>2</sub>CO<sub>3</sub> particles. To confirm the speculation, the

cycling runs in the photodegradation of MO by  $\text{Ag}_2\text{CO}_3$  in the presence of  $\text{CO}_3^{2-}$  were performed as shown in Fig.SI 3. After the addition of  $\text{CO}_3^{2-}$ , the stability of  $\text{Ag}_2\text{CO}_3$  was significantly improved. It can be inferred that the dissolution of  $\text{Ag}_2\text{CO}_3$  should be partially responsible for the unstability of  $\text{Ag}_2\text{CO}_3$  thus proved our speculation indirectly.

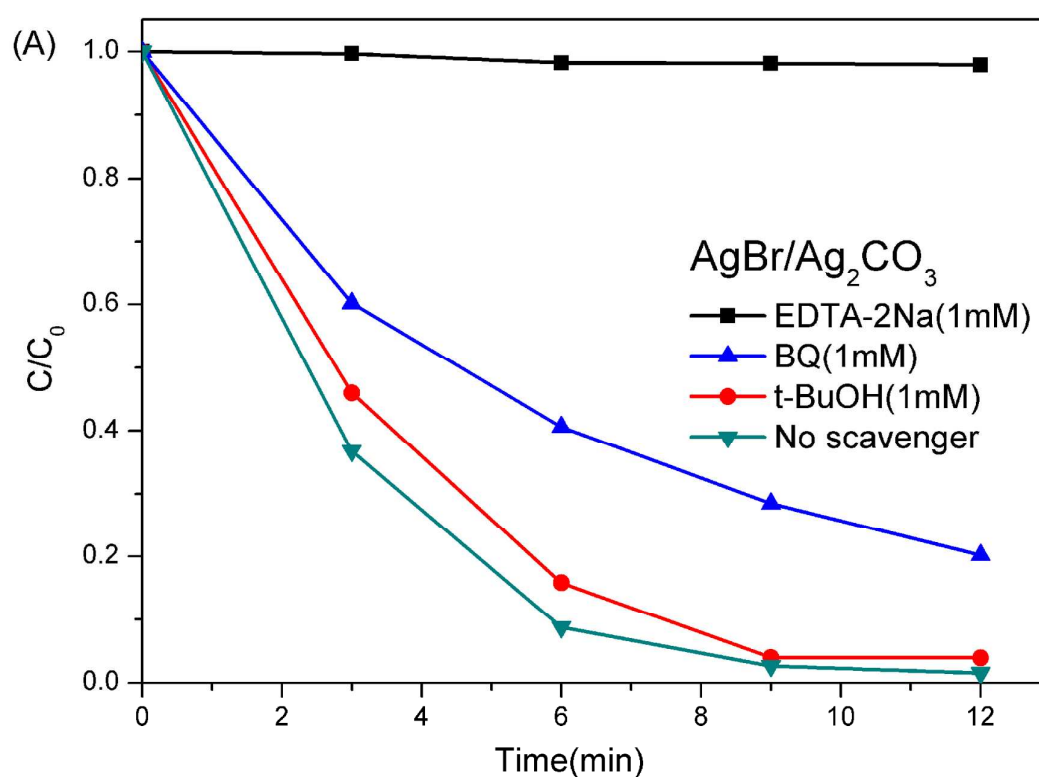
### 3.5 Photocatalytic mechanism of AgBr/ $\text{Ag}_2\text{CO}_3$

#### 3.5.1 Band structure calculation

For photocatalysts, their band structures have conspicuous influence upon the photocatalytic performance. Furthermore, the transfer direction of photo-generated charge carriers in hybrids depends on the relative band position of the component. Thus, the band edge positions of the conduction band and the valence band for AgBr and  $\text{Ag}_2\text{CO}_3$  were calculated using the atom's Mulliken electronegativity equation:  $E_{CB} = \chi - E^e - 0.5E_g$ . Where  $\chi$  is the absolute electronegativity of the semiconductor,  $E^e$  is the energy of free electrons on the hydrogen scale (4.5 eV), and  $E_g$  is the band gap of the semiconductor. Consequently, the bottom of conduction band  $E_{CB}$  for AgBr and  $\text{Ag}_2\text{CO}_3$  were estimated to be 0.11 eV and 0.39 eV, respectively. The top of valence band were calculated using  $E_{VB} = E_{CB} + E_g$ . The  $E_{VB}$  values were calculated to be 2.49 eV and 2.64 eV for AgBr and  $\text{Ag}_2\text{CO}_3$ , respectively.

### 3.5.2 Activated species detection

It is generally accepted that photo-generated holes,  $\cdot\text{OH}$  and  $\cdot\text{O}_2^-$  are the main reactive species in the photocatalytic process. To verify the role of these reactive species, EDTA-2Na, *tert*-butanol (t-BuOH) and benzoquinone (BQ) were introduced into  $\text{Ag}_2\text{CO}_3$ -based photocatalytic degradation process as scavengers for  $\text{h}^+$ ,  $\cdot\text{OH}$  and  $\cdot\text{O}_2^-$ , respectively.<sup>28,29</sup>



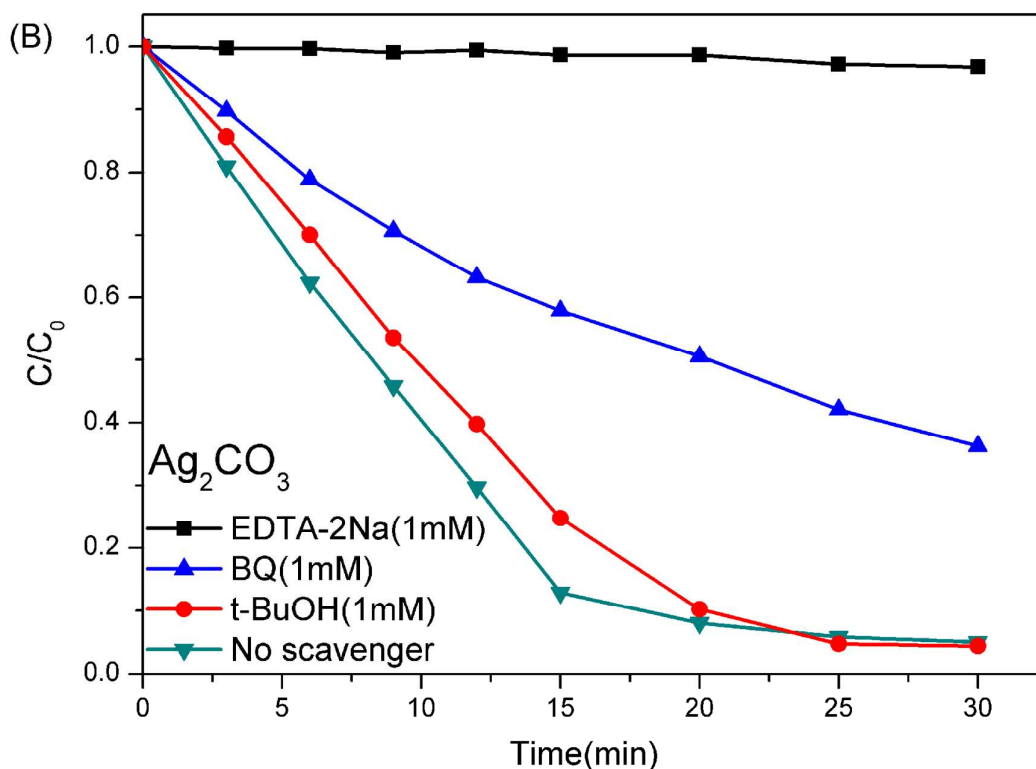


**Fig 8. Photocatalytic degradation of MO under visible light in presence of different scavengers over AgBr/Ag<sub>2</sub>CO<sub>3</sub>-60% (A) and Ag<sub>2</sub>CO<sub>3</sub> (B).**

As illustrated in Fig.8A, with regard to the AgBr/Ag<sub>2</sub>CO<sub>3</sub>-60% system, the addition of t-BuOH had little impact on the photocatalytic degradation of MO. On the contrary, the photocatalytic activity of AgBr/Ag<sub>2</sub>CO<sub>3</sub>-60% was almost completely suppressed after the addition of EDTA-2Na. It suggested that there was no •OH radical involved in the photocatalytic process and the holes were the dominant oxidative species. Moreover, the addition of BQ decreased the degradation efficiency of MO indicating the existence of •O<sub>2</sub><sup>-</sup>. The similar tendency was found in Ag<sub>2</sub>CO<sub>3</sub> system as shown in Fig 8B.

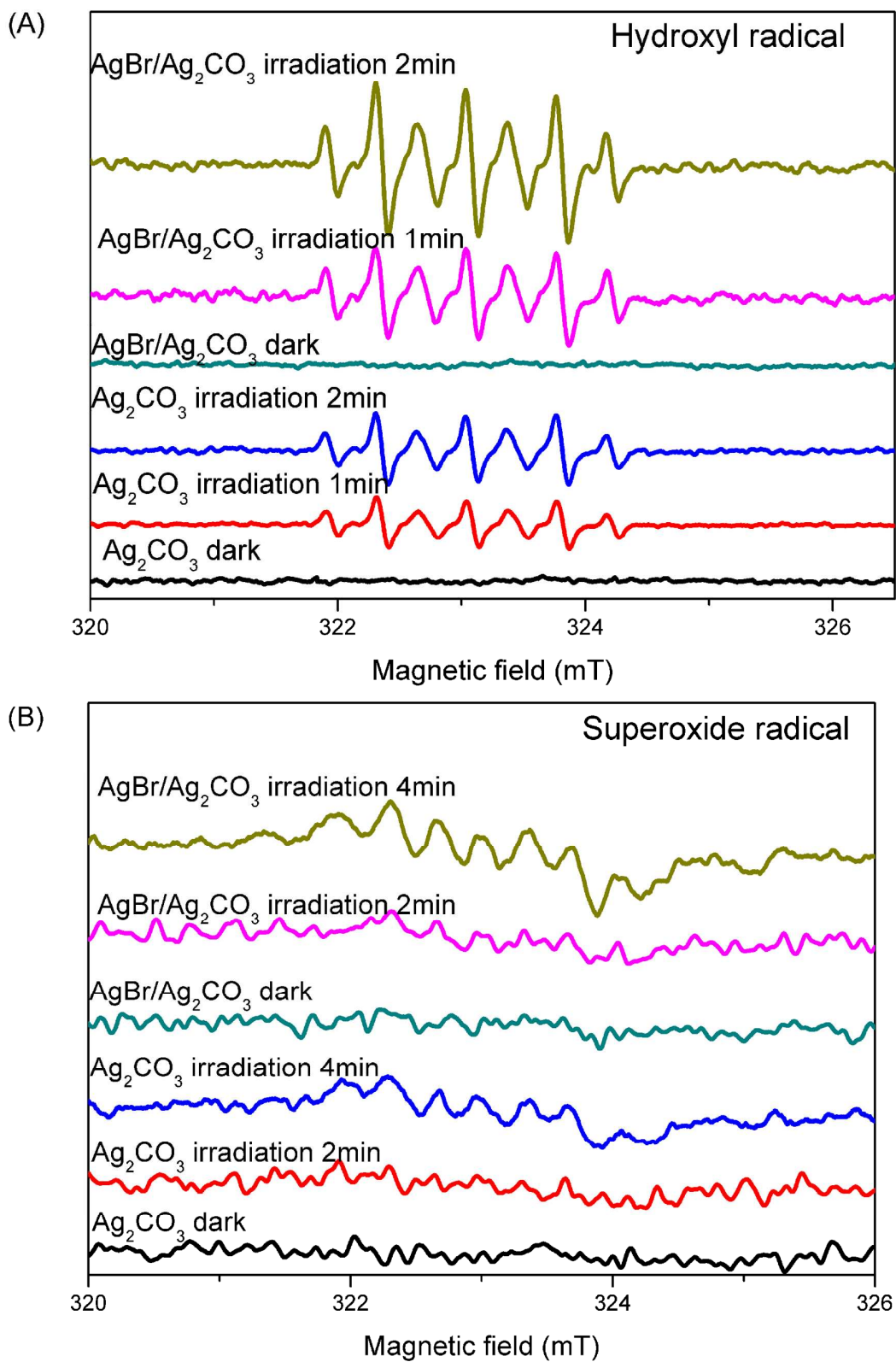


Fig 9. DMPO spin-trapping ESR spectra of Ag<sub>2</sub>CO<sub>3</sub> and AgBr/Ag<sub>2</sub>CO<sub>3</sub>-60% in

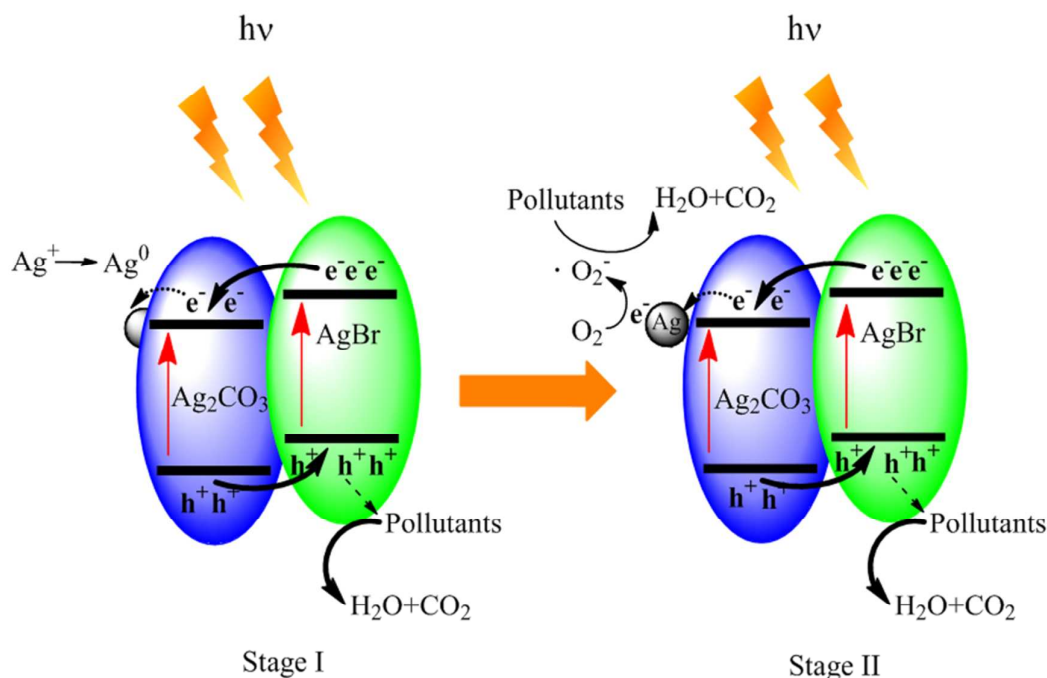
darkness and under visible light irradiation ( $\lambda > 420$  nm) for DMPO- $\bullet$ OH in aqueous dispersion (A) and for DMPO- $\bullet$ O<sub>2</sub><sup>-</sup> in methanol dispersion (B).

However, Mehraj<sup>15</sup> reported that  $\bullet$ OH was the primary reactive specie in AgBr/Ag<sub>2</sub>CO<sub>3</sub> system on the degradation of PBS and it is not possible to generate  $\bullet$ O<sub>2</sub><sup>-</sup> by AgBr/Ag<sub>2</sub>CO<sub>3</sub> which was in conflict with our finding. Thus, to further confirm whether there were  $\bullet$ OH and  $\bullet$ O<sub>2</sub><sup>-</sup> in detail, an ESR spin-trap technique with DMPO was employed. As shown in Fig 9A, no characteristic four peaks of DMPO- $\bullet$ OH with intensity 1:2:2:1 appeared in either Ag<sub>2</sub>CO<sub>3</sub> or AgBr/Ag<sub>2</sub>CO<sub>3</sub> photocatalyst before or after irradiation. It confirmed the absence of  $\bullet$ OH radicals in photocatalytic process. Instead, the hyperfine splitting peaks with an intensity ratio 1:2:1:2:1:2:1 were detected under illustration. According to the report from Dikalov,<sup>30</sup> this signal is attributed to DMPOX, which is a direct oxidized product from DMPO. Since no peaks were found in dark condition, the production of DMPOX under visible light could be ascribed to the direct oxidation by h<sup>+</sup>.<sup>31</sup> The intensities of DMPOX generated in AgBr/Ag<sub>2</sub>CO<sub>3</sub> suspension were much greater than those in Ag<sub>2</sub>CO<sub>3</sub>. It indicated that AgBr/Ag<sub>2</sub>CO<sub>3</sub> composite produced larger amount of h<sup>+</sup> than Ag<sub>2</sub>CO<sub>3</sub> in photocatalytic process which is consistent with the stronger photocatalytic degradation ability of AgBr/Ag<sub>2</sub>CO<sub>3</sub> composite mentioned above. As illustrated in Fig 9B, characteristic peaks of DMPO- $\bullet$ O<sub>2</sub><sup>-</sup> were observed in both Ag<sub>2</sub>CO<sub>3</sub> and AgBr/Ag<sub>2</sub>CO<sub>3</sub>

composites which confirmed the existence of  $\bullet\text{O}_2^-$  under visible light irradiation. The signals were stronger in the presence of AgBr/Ag<sub>2</sub>CO<sub>3</sub> composites than pure Ag<sub>2</sub>CO<sub>3</sub>. It is seen that both characteristic peak intensities of DMPOX and DMPO- $\bullet\text{O}_2^-$  increased with irradiation time for Ag<sub>2</sub>CO<sub>3</sub> and AgBr/Ag<sub>2</sub>CO<sub>3</sub> composites. However, it is notable that it took 2 minutes for the characteristic peak intensities of DMPOX to reach its maximum while it took 6 minutes for those of DMPO- $\bullet\text{O}_2^-$ . It implied that the formation of  $\bullet\text{O}_2^-$  lagged behind  $h^+$ . These results clearly indicate that active species  $h^+$  and  $\bullet\text{O}_2^-$  contribute most to the photocatalytic system, rather than  $\bullet\text{OH}$  did.

However, it is interesting that the  $E_{\text{CB}}$  potentials of Ag<sub>2</sub>CO<sub>3</sub> or AgBr is more positive than  $E_0(\text{O}_2/\bullet\text{O}_2^-)$  (-0.046 eV vs NHE)<sup>28</sup> which means that the electrons on the conduction band of Ag<sub>2</sub>CO<sub>3</sub> or AgBr cannot reduce O<sub>2</sub> to  $\bullet\text{O}_2^-$ . In consideration of the formation of Ag<sup>0</sup> on AgBr/ Ag<sub>2</sub>CO<sub>3</sub> as discussed above, we believe that the  $\bullet\text{O}_2^-$  radicals were generated by the electrons from the surface of Ag NPs. Similar phenomenon have been reported in Ag/ AgVO<sub>3</sub> and Ag/AgCl systems.<sup>27,32</sup>

### 3.5.3 Possible photocatalytic degradation mechanism



**Scheme 1. Schematic illustration of two-stage photocatalytic mechanism within AgBr/Ag<sub>2</sub>CO<sub>3</sub> system under visible light irradiation.**

On the basis of band structure calculation, experimental results, DMPO spin-trapping ESR spectra as well as related literature work, the photocatalytic mechanism of AgBr/Ag<sub>2</sub>CO<sub>3</sub> composite was proposed as illustrated in scheme 1. The photocatalytic process was divided into two stages according to the different reaction pathway of photo-generated electron. At the first stage, when exposed to visible light irradiation, both AgBr and Ag<sub>2</sub>CO<sub>3</sub> were excited leading to the generation of electron-hole pairs. Considering the more negative conduction band position of AgBr and the more positive valence band position of Ag<sub>2</sub>CO<sub>3</sub>, the photoinduced electrons in AgBr would migrate to the conduction band of Ag<sub>2</sub>CO<sub>3</sub> while h<sup>+</sup> would transfer from valence band of Ag<sub>2</sub>CO<sub>3</sub> to that of AgBr. This

could help the separation of electron-hole pairs. The holes oxidized the pollutants directly as the most important oxidants. The accumulated electrons in  $\text{Ag}_2\text{CO}_3$  would self-reduce the interstitial silver ions leading to the formation of Ag nanoparticles (Ag NPs). Therefore, the  $\text{AgBr}/\text{Ag}_2\text{CO}_3$  system was turned to  $\text{AgBr}/\text{Ag}/\text{Ag}_2\text{CO}_3$  system. In the newly constructed photocatalytic system, due to the polarization effect of the negatively charged  $\text{Ag}_2\text{CO}_3$  surface,<sup>33</sup> the photo-generated electrons would immigrate to the surface of Ag NPs rather than  $\text{Ag}_2\text{CO}_3$  resulting in the aggregation of electrons on Ag NPs. At the second stage, when the holes continued to oxidize pollutants, the electrons on Ag NPs were trapped by surface adsorbed  $\text{O}_2$  to form  $\cdot\text{O}_2^-$  which began to participate in degradation of pollutants. This was consistent with the results mentioned above that the generation of  $\cdot\text{O}_2^-$  lagged behind that of  $\text{h}^+$  and the addition of BQ inhibited the photocatalytic degradation efficiency. Furthermore, the consumption of  $\text{e}^-$  on Ag NPs could stabilize the  $\text{AgBr}/\text{Ag}/\text{Ag}_2\text{CO}_3$  system.

#### 4. Conclusions

In summary,  $\text{AgBr}/\text{Ag}_2\text{CO}_3$  photocatalyst was synthesized through simple ion-exchange process. The hybrid displayed excellent degradation ability on methyl orange (MO), tetracycline (TC) and bisphenol A (BPA) compared to pure  $\text{Ag}_2\text{CO}_3$ , and  $\text{AgBr}/\text{Ag}_2\text{CO}_3$ -60% exhibited the most

effective photocatalytic activity. It was found that AgBr/Ag<sub>2</sub>CO<sub>3</sub> showed enhanced stability which could keep 90.4% of methyl orange degradation in 20 min after the fifth run. Such improvement in stability might be resulted from the formation of AgBr/Ag/Ag<sub>2</sub>CO<sub>3</sub> system as well as the decreased dissolved quantity of Ag<sub>2</sub>CO<sub>3</sub> achieved by AgBr coating. On the basis of radical-trapping experiments and ESR tests, h<sup>+</sup> and •O<sub>2</sub><sup>-</sup> were found to be the main reactive species responsible for the degradation of pollutants. Photocatalytic process of AgBr/Ag<sub>2</sub>CO<sub>3</sub> could be divided into two stages. In stage I, the photo-generated electrons were trapped by Ag<sup>+</sup> to form Ag<sup>0</sup>. In stage II, the electrons reacted with O<sub>2</sub> on the surface of Ag<sup>0</sup>. During the photocatalytic process, the h<sup>+</sup> could be generated in both stages while •O<sub>2</sub><sup>-</sup> could only be produced in the second one. We expect that the two-stage theory would provide new insight for revealing the underlying photocatalytic mechanism for Ag-based photocatalysts.

## 5. Acknowledgments

This work is supported by National Major Science and Technology Program for Water Pollution Control and Treatment of China (No. 2014ZX07101-012).

## References

- 1 S. Ge and L. Zhang, *Environ. Sci. Technol.*, 2011, **45**, 3027.
- 2 H. Cheng, B. Huang, P. Wang, Z. Wang, Z. Lou, J. Wang, X. Qin, X. Zhang and Y. Dai, *Chem. Commun.*, 2011, **47**, 7054.
- 3 X. Li, P. Zhang, L. Jin, T. Shao, Z. Li and J. Cao, *Environ. Sci. Technol.*, 2012, **46**, 5528.
- 4 H. Chen, S. Chen, Q. Xie, Y. Zhang, *Environ. Sci. Technol.*, 2010, **44**, 451.
- 5 X. Li, X. Zhen, S. Meng, J. Xian, Y. Shao, X. Fu and D. Li, *Environ. Sci. Technol.*, 2013, **47**, 9911.
- 6 G. Li, Y. Wang and L. Mao, *RSC Adv.*, 2014, **4**, 53649.
- 7 Z. Yi, J. Ye, N. Kikugawa, T. Kako, S. Ouyang, H. S. Williams, H. Yang, J. Cao, W. Luo, Z. Li, Y. Liu and R. L. Withers, *Nat. Mater.*, 2010, **9**, 559.
- 8 C. Xu, Y. Liu, B. Huang, H. Li, X. Qin, X. Zhang and Y. Dai, *Appl. Surf. Sci.*, 2011, **257**, 8732.
- 9 C. Feng, G. Li, P. Ren, Y. Wang, X. Huang and D. Li, *Appl. Catal. B*, 2014, **158-159**, 224.
- 10 C. Wu, *Mater. Lett.*, 2014, **136**, 262.
- 11 C. Yu, G. Li, S. Kumar, K. Yang and R. Jin, *Adv. Mater.*, 2014, **26**, 892.
- 12 G. Dai, J. Yu and G. Liu, *J. Phys. Chem. C*, 2012, **116**, 15519.
- 13 H. Dong, G. Chen, J. Sun, Y. Feng, C. Li, G. Xiong and C. Lv, *Dalton T.*, 2014, **43**, 7282.
- 14 H. Xu, J. Zhu, Y. Song, W. Zhao, Y. Xu, Y. Song, H. Ji and H. Li, *RSC Adv.*, 2014, **4**, 9139.
- 15 O. Mehraj, N. A. Mir, B. M. Pirzada, S. Sabir and M. Muneer, *J. Mol. Catal. A: Chem.*, 2014, **395**, 16.
- 16 X. Yao and X. Liu, *J. Hazard Mater.*, 2014, **280**, 260.
- 17 J. Wang, C. Dong, B. B. Jiang, K. L. Wu, J. Sun, X. Z. Li, W. J. Zhang, B. Zhang and X. W. Wei, *Mater. Lett.*, 2014, **131**, 108.

- 18 C. Dong, K. L. Wu, X. W. Wei, X. Z. Li, L. Liu, T. H. Ding, J. Wang and Y. Ye, *CrystEngComm*, 2014, **16**, 730.
- 19 H. Fei, W. Leng, X. Li, X. Cheng, Y. Xu, J. Zhang and C. Cao, *Environ. Sci. Technol.*, 2011, **45**, 4532.
- 20 H. Dong, G. Chen, J. Sun, C. Li, Y. Yu and D. Chen, *Appl. Catal. B*, 2013, **134-135**, 46.
- 21 J. Cao, B. Luo, H. Lin and S. Chen, *J. Mol Catal A: Chem.*, 2011, **344**, 138.
- 22 H. Xu, Y. Xu, H. Li, J. Xia, J. Xiong, S. Yin, C. Huang and H. Wan, *Dalton T.*, 2012, **41**, 3387.
- 23 L. Kong, Z. Jiang, H. H. Lai, R. J. Nicholls, T. Xiao, M. O. Jones and P. P. Edwards, *J. Catal.*, 2012, **293**, 116.
- 24 J. Cao, B. Luo, H. Lin and S. Chen, *J Hazard Mater*, 2011, **190**, 700.
- 25 Y. Liu, L. Fang, H. Lu, Y. Li, C. Hu and H. Yu, *Appl. Catal. B*, 2012, **115-116**, 245-252.
- 26 H. Zhang, G. Wang, D. Chen, X. Lv and J. Li, *Chem. Mater.*, 2008, **20**, 6543.
- 27 W. Zhao, Y. Guo, Y. Faiz, W. T. Yuan, C. Sun, S. M. Wang, Y. H. Deng, Y. Zhuang, Y. Li, X. M. Wang, H. He and S. G. Yang, *Appl. Catal. B.*, 2015, **163**, 288.
- 28 Z. Chen, W. Wang, Z. Zhang and X. Fang, *J. Phys. Chem. C*, 2013, **117**, 19346.
- 29 F. T. Li, X. J. Wang, Y. Zhao, J. X. Liu, Y. J. Hao, R. H. Liu and D. S. Zhao, *Appl. Catal. B*, 2014, **144**, 442.
- 30 S. I. Dikalov and R. P. Mason, *Free Radical Bio. Med.*, 2001, **30**, 187.
- 31 Y. Zhou, X. Zhang, Q. Zhang, F. Dong, F. Wang and X. Zhuo, *J. Mater. Chem. A*, 2014, **2**, 16623.
- 32 R. Dong, B. Tian, C. Zeng, T. Li, T. Wang and J. Zhang, *J. Phys. Chem. C*, 2013, **117**, 213.
- 33 X. Jin, I. Y. Kim, Y. K. Jo, J. L. Bettis, H.-J. Koo, M.-H. Whangbo and S.-J. Hwang, *J. Phys. Chem. C*, 2013, **117**, 26509.

